www.cadanda.com
Computer-Aided Design AND APPLICATIONS

Mesoscale Modeling of Aluminum Foams for FEA of Scattering Effects due to Cell Distribution

Michele Bici[1], Francesca Campana[2], Edoardo Mancini[3], Daniela Pilone[4] and Marco Sasso[5]

[1]Sapienza University of Rome, michele.bici@uniroma1.it
[2]Sapienza University of Rome, francesca.campana@uniroma1.it
[3]Università degli studi L'Aquila, edoardo.mancini@univaq.it
[4]Sapienza University of Rome, daniela.pilone@uniroma1.it
[5]Università Politecnica delle Marche, m.sasso@staff.univpm.it

Corresponding author: Francesca Campana, francesca.campana@uniroma1.it

Abstract. Mechanical behavior of metallic foams suffers from scattering due to morphology and distribution of cells. FEA modeling, at mesoscale level, may assist design of metallic foam components or the development of a proper model able to consider the effects of this variability. This paper discusses a foam modeling approach based on a surface tessellation provided by a Voronoi diagram, investigating its ability to obtain a final model that respects an assigned cell morphology. Results show that a wide range of void volume fraction can be achieved, with good agreement between assigned cell morphology and modeled cell distribution. Absence of non-manifold geometry and STL optimization speed-up the FEA checks on the solid mesh creation, so that, many models may be systematically simulated to investigate the role of cell morphology during deformation.

Keywords: Aluminum foam, Mesoscale geometric modeling, Voronoi Diagram, FEA, Non-linear analysis.
DOI: https://doi.org/10.14733/cadaps.2021.1296-1305

1 INTRODUCTION

Mechanical behavior of metallic foams is strictly related to relative density calculated in relation to their bulk materials [4,10]. Under compression, void distribution (stochastic or regular) and cell morphology (open or closed cell, aspect ratio, …) affect also the progressive local behavior, inducing scattering on the load-displacement curves [12,14]. Finite Element Analysis (FEA) may support the analysis of cell effects and may help to quantify the scattering related to the characteristics of cell morphology. Manufacturing process controls the relative density and may also affect cell shape and roundness [3]. Figure 1 shows the difference between foams made by powder compacts and infiltration processes. In the first case, Figure 1(a), roundness is more evident, while, in the second

one, Figure 1(b), size and shapes are related to the shape of salt grains selected for the production of the leachable preform.

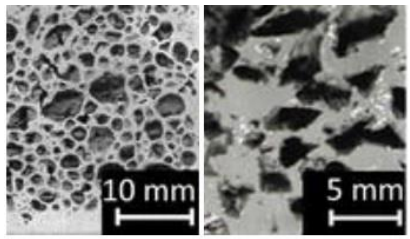

Figure 1: Macrographs showing the morphology of: (a) Closed Cells obtained by powder compacts, (b) Open Cells obtained by infiltration process.

Different authors presented works on structural simulations of foam structures, both in the fields of geometrical modeling and simulation. Geometrical modeling of mesoscale porosity needs to reproduce patterns, according to Voronoi diagrams, or unit cell replication (e.g., Kelvin cell structure) through proper space filling strategies [1,13]. Voronoi diagrams are convenient for cells with stochastic distributions like those present in metallic foams. Shared library like Voro++ or commercial add-ons, like Voronoi Sketch generator, may help to model mesoscale structures with different complexity. In [2], examples of how mesoscale modeling may describe the effective behavior of foams in mechanical tests are provided, together with two approaches for achieving FEA models from experimental morphological data. One approach is based on Voronoi cells, the other on Reverse Engineering based on reconstruction of cut sections or tomography, that now is becoming more widespread [15].

In [14], a modeling strategy based on Voronoi cell distribution and an analysis of sensitivity to the computational parameters have been discussed. More in detail, the effects of cell thickness are treated, according to the sensitivity to numerical parameters necessary in explicit FEA set-up (mass scaling, element size). In [5,7], mesoscopic models investigate the effect of impact velocity, material strength and porosity distribution on energy absorption of metallic foams. Under plastic deformation, local strain distributions at specific cells can affect the global collapse of the specimens, increasing the scattering of the global indicators of the mechanical behavior (e.g., stress-strain curves or strain rate effects).

This paper discusses the definition of a geometric modeling workflow that achieves FEA models of foam specimens with imposed morphological cell distributions. Starting from the Voronoi diagram approach presented in [2], it analyses how the steps in the modeling workflow may introduce geometrical approximation errors that change the nominal cell conditions, so that, limits of applicability and proper solutions may be outlined. After the recap of the modeling workflow in Section 2, Section 3 describes the sensitivity analysis to the modeling steps and theirs related parameters. Then, in Section 4, some results achieved by FEA show how the modeling tool and its parameters affect the mechanical behavior. Finally, in Section 5, Conclusion are discussed.

2 MODELING WORKFLOW

Mesoscale FEA modeling of foams may be carried out adopting solid or shell meshes, in conformity to the averaged ratio between cell area and its wall thickness. In both cases, computational efforts and quality of the results are strictly related to mesh quality (density, aspect ratio, warpage, ….) and control parameters, both with implicit (e.g., Optistruct, Ansys, Abaquus implicit, …) and explicit codes (e.g., Radioss, LS-Dyna, Abaquus explicit). In both cases, a surface mesh of the cells must be conveniently defined starting from:

- Relative density, ρ/ρ_0 , of the foam (where ρ_0 stands for the density of the bulk material),

- statistical distribution of cells, defined in terms of cell area, *A*, roundness, *R*, and presence or not of a bulk outer wall, mainly due to the alloy solidification in the die,
- specimen section and length, so that the reference volume, *V*, can be defined.

Figure 2 provides an example referred to a single slice cut from a specimen produced by means of powder compact process. Figure 2(a) shows a macrograph of a foam specimen transversal section; Figures 2(b) and 2(c) show the image segmentations regarding the cell size and roundness analysis, respectively. In Figure 3, histograms of the distributions of cell size, 3(a), and roundness, 3(b), are reported. According to the experimental conditions and resources, statistical distributions of the cell morphology may be evaluated through cuts on assigned slices of the specimens or through non-destructive tests like tomography.

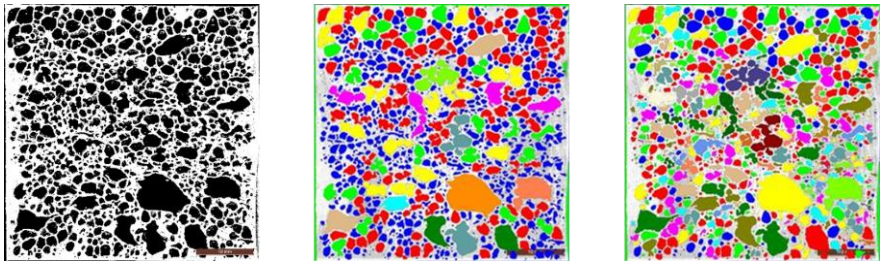

Figure 2: (a) Foam specimen transversal section (b) image segmentation achieved for cell size analysis, (c) image segmentation achieved for cell roundness analysis.

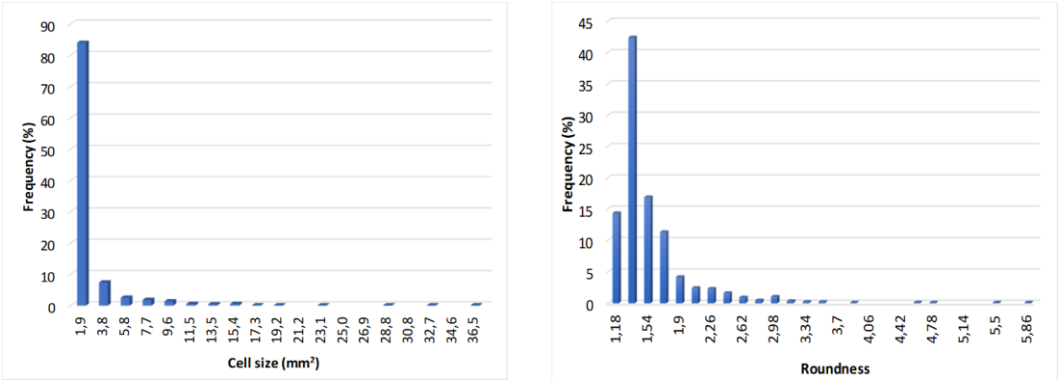

Figure 3: Foam cell morphology evaluation through image analysis carried out on transversal sections: (a) cell size distribution, (b) cell roundness distribution.

The proposed modeling workflow has been implemented in MATLABR2019b, and it is organized in 3 steps: (1) definition of the initial cell structure; (2) cell structure updating according to cell morphology descriptors (cell size and roundness); (3) mesh length optimization and FEA meshing.

2.1 Definition of the Initial Cell Structure

The first step of the workflow defines the reference volume, V, with a set of N seeds suitable to position the cells. N is defined so that V is supposed to be filled by regular spheres able to guarantee a Void Volume Fraction, VVF= $1-\rho/\rho_0$:

$$N = floor\left(VVF \cdot \frac{V}{V_{sphere}}\right) \tag{2.1}$$

$$V_{sphere} = \frac{4}{3} \cdot \pi \cdot r^2 \tag{2.2}$$

where *r* stands for the cell mean radius as derived from foam cell size distribution, and V_{sphere} for the volume of a single regular cell.

Seed positions, Figure 4(a), are random in V, although they can be conveniently spaced in cluster adopting algorithm such as the Simple Sequential Inhibition Process (SSIP). Function *floor* is used in Equation (2.1) to simply provide a uniform truncation in each case. The Voronoi diagram associated to seeds represents the initial cell structure. It has cells randomly distributed with different elongations and sizes in accordance with the geometrical properties related to the Voronoi diagram theory [6,8,9,14]. This initial cell structure must be iteratively improved, through the cell structure updating, so that the final statistical distribution of the cells agrees with the experimental input.

2.2 Cell Structure Updating

First, the Voronoi diagram is converted into a tessellated space along the vertexes, excluding open cell at the boundary. They are found through the *Inf* value assumed at least in one of their vertexes, since the *Inf* value represents the open cell provided in Matlab. Then closed cells are measured in terms of an equivalent radius (as the average distance from cell center and vertexes) and roundness (here applied as the ratio between actual cell volume and equivalent sphere with average radius). Cell filter on roundness is applied adopting a threshold proportional to the standard deviation, σ, experimentally evaluated. Doing so the experimental distribution of the cell morphology is associated to the mean and standard deviation of cell size and roundness. This step typically excludes elongated cells concentrated nearby the edge of the specimen, Figure 4(b). As a drawback, excluding cells, this step reduces the effective VVF, so that, an effective void volume, V_{0eff} , must be defined and optimized with respect to the nominal one:

$$V_0 = VVF \cdot V \tag{2.3}$$

As better described in section 3, the initial cell structure overestimates the V_0 since seeds are associated to cells equivalent to the Voronoi diagram. On the contrary, the threshold on the roundness reduces V_{0eff}. In practice, this makes possible a scaling of the cells (through a factor that in section 3 is named X), able to reduce their volume, so that, the difference between V_{0eff} and V_0 is minimized, as in Figure 4(c).

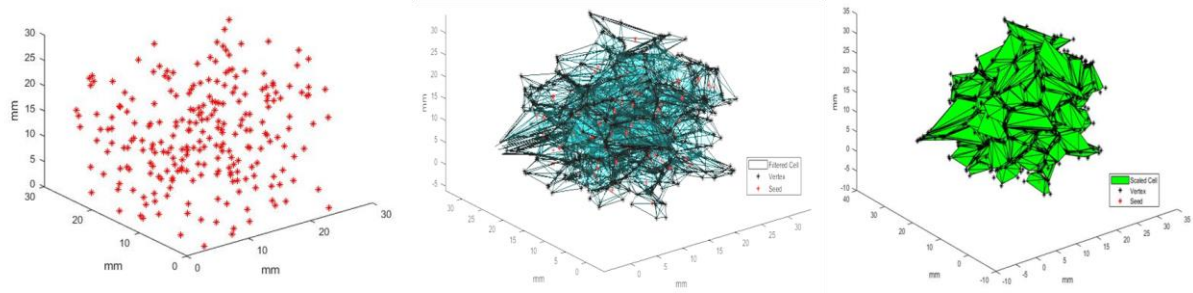

Figure 4: Cell generation: (a) seeds, (b) filtered cells from Voronoi diagram, (c) scaled cells after filtering.

The Voronoi Diagram provides an "STL" convex tessellation of the cells that cannot be directly applied as FEA model, since a proper tetrahedral mesh of the filled volume must be created and optimized (a shell mesh can also be derived but it has been considered beyond the scope of this work).

2.3 Mesh Length Optimization and FEA Meshing

The tetrahedral mesh may be built in two ways:

1. as a tetramesh, starting from regular surface meshes of the cells and of the external edges of the specimen;
2. as a tetramesh of the overall volume defined from the boundary surfaces of the cells and of the specimen.

The first method can be carried out starting from an optimized re-meshing of the tessellation of the cell outer surfaces; the second method requires a surface fitting of the cells and their selection to define the overall volume to be meshed.

To avoid time-consuming FEA pre-processing activities, and mesh errors in possible critical areas (non-manifold local meshes or missing elements, for example), the first approach is here selected and discussed. After an integrity check to avoid non-manifold vertexes or overlapping, the STL convex tessellation is optimized for FEA, modifying mesh parameters in terms of dihedral angle (30°), and uniformity of length (Figure 5(a)). This will induce a smoothing effect that must be checked and, if necessary, mitigated (Figure5(b)).

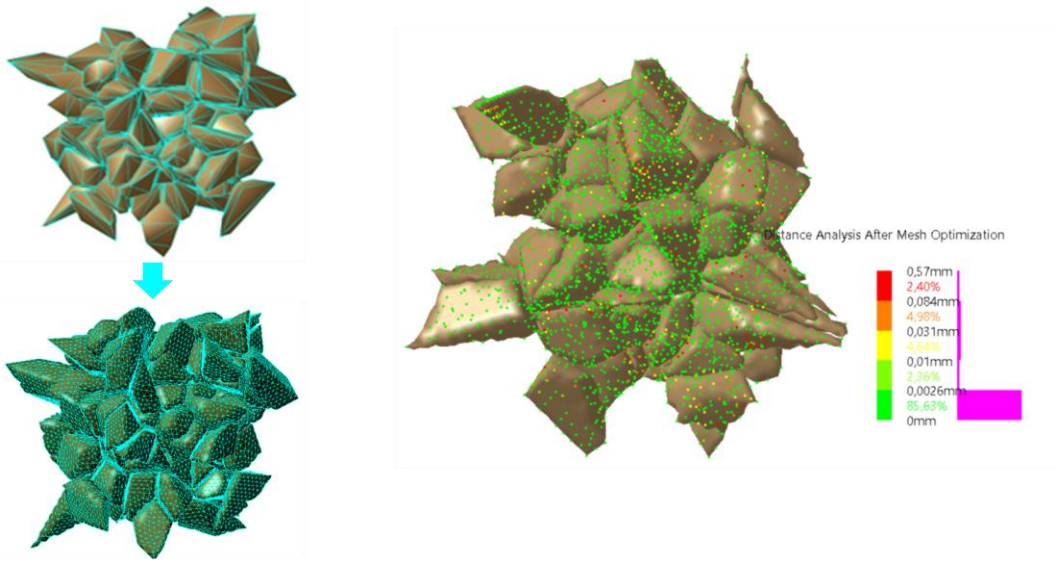

Figure 5: FEA modeling: (a) Surface mesh optimization, (b) Distance Analysis between original and the optimized mesh.

Although Figure 3 shows few bars with high values of frequency around mean values, outliers may make the difference. As shown in Figure 1(a), some larger cells are present and, as it will be shown in Section 4, they provide major chances of stress localization and not uniform deformation under compression, thus producing scattering in mechanical behavior. Outlier cells, in term of size, can be inserted through post-processing of the Voronoi diagram. Through random selection or index selection, one or more cells can be selected and collapse on their neighbors iteratively, checking the constraint related to the final VVF.

3 SENSITIVITY ANALYSIS

The FEA models derived from the proposed workflow meant to represent foams with random cell morphology like an assigned distribution found experimentally, not exactly replicate it. Although its implementation in Matlab2019 is based on an agile script able to generate thousands of cells in no more than few minutes (with an Intel(R) Core (TM) i7 -8565U CPU @1.80GHz), the evaluation of the final cell statistic must be checked in the respect of the cell structure updating and the mesh length optimization.

Cell size distribution is related to initial cell structure, as described in the previous Section 2.1. Equations (2.1) and (2.2) assume that the VVF is distributed along regular spheres with radius equal to the mean experimental value of the cell radius. The adoption of the Voronoi Diagram associated to seeds as initial cell structure has the advantage of guaranteeing no cell overlapping, intersection or degeneration. On the contrary, together with a natural dispersion on the cell size, that is one of the requirements to be achieved, it may introduce very elongated cells, often nearby the boundaries of V. This is managed through the cell structure updating, by analyzing the roundness of the cells. Table 1 shows the achieved results changing cell area, sphericity, and N, by applying a scale factor for V, assuming that the updating of cells at the boundaries may be compensated by enlarging V through a factor X. Results show that a wide range of VVF_{eff} can be achieved changing X, although its max and min values are function of Cell area and sphericity. This confirms the role of threshold in the final number of cells within the volume V. Figure 6 shows the trends of VVF_{eff} presented in Table 1 as parametric graphs of cell size and sphericity. No interaction with X is present. These results are achieved starting with a nominal value of VVF of 0.4. Similar trends occurs with nominal values of VVF in the range [0.7÷0.3].

Input				*Output*		
Cell area (mm^2)	*Sphericity*	*X*	*N*	*No. Of cells*	*Void Volume (mm^3)*	*VVF_{eff}*
1.6	5	1	2067	1567	30758.60	0.99
		1.3	2687	2176	12219.60	0.62
	3	1	2067	1133	23560.33	0.99
		1.3	2687	2185	12262.1	0.62
1.9	5	1.0	1598	1169	14563.00	0.93
		1.2	1917	1502	15938.00	0.50
		1.25	1997	1602	16581.00	0.42
		1.3	2077	1649	16335.90	0.36
		1.4	2237	1815	16654.70	0.28
	3	1.0	1598	815	8009.80	0.71
		1.2	1917	1265	11286.00	0.46
		1.25	1997	1327	11720.00	0.38
		1.3	2077	1440	16335.90	0.31
		1.4	2237	1550	16654.70	0.23
2.2	5	1.0	1282	928	11802.2	0.60
		1.3	1666	1306	4306.1	0.22
	3	1.0	1282	652	9558.80	0.49

		1.3	1666	1108	3923.50	0.20

Table 1: No. of cells, V_{0eff}, VVF_{eff} in function of Cell area, Sphericity and N.

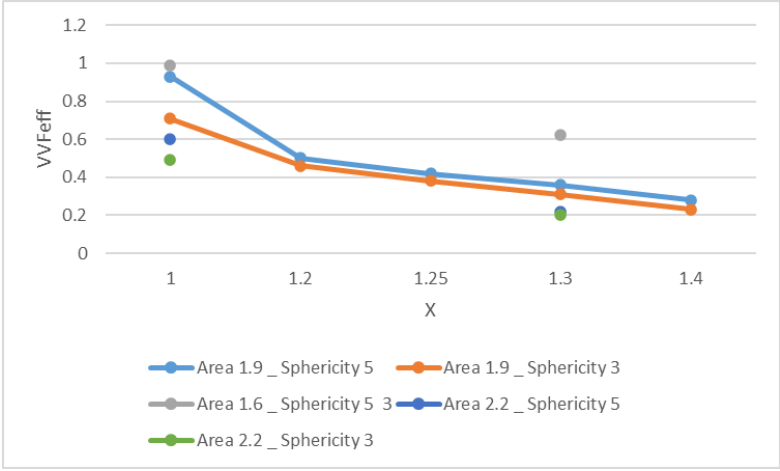

Figure 6: Interaction effect of Cell Area and Sphericity with X on VVF_{eff}.

Figures 7 and 8 highlight specific results for the case nearest to the nominal condition VVF = 0.4. Figure 7 shows the morphological distribution of cells.

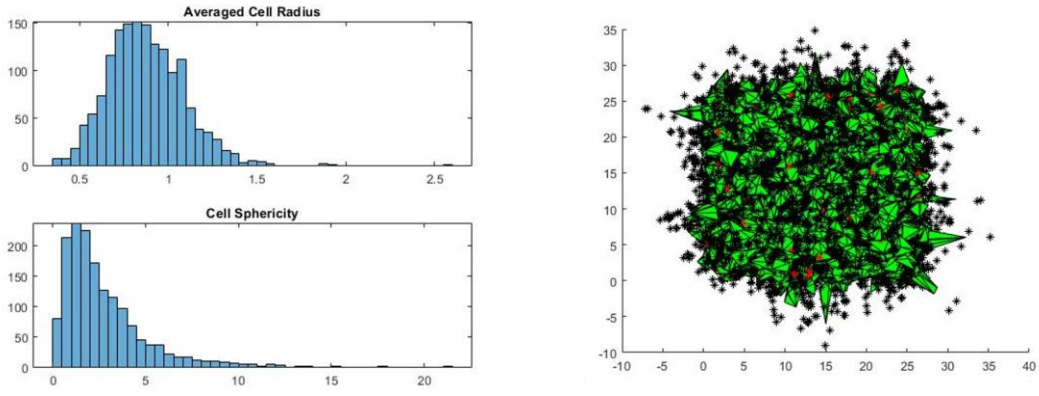

Figure 7: X = 1.25, Cell Size = 1.9 mm^2, Sphericity = 5, 1602 cells: (a) distributions of cell morphology, (b) scaled cells after filtering.

Concerning the mesh optimization, maintaining the minimum length in the same range of the cell radius, it allows to reduce major smoothing effects, as shown through the distance analysis of Figure 5(b) and Figure 8(b). They are obtained as distance analyses among points of the original STL (used as reference) and the one obtained with mesh optimization (min length equal to 0.5 mm). Figure 8(a) highlights the difference between the two tessellations showing two halves together.

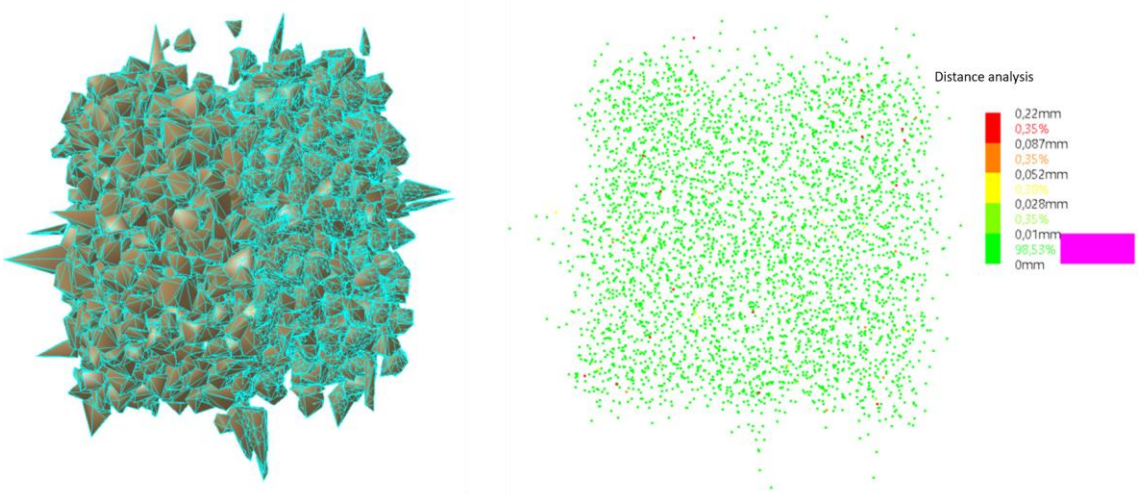

Figure 8: (a) Tessellation before and after mesh optimization, (b) distance analysis after mesh optimization.

In this case, Figures 7 and 8 highlight also the presence of elongated cells, especially nearby the edges.

4 FEA ANALYSIS

From the optimized STL, the model can be imported in a FEA solver (in our case, Radioss in Altair Hyperworks suite), so that, tetramesh can be generated and simulation may run. Figure 9 shows the final model, 9(a), and two sections: one, 9(b), referred to the original model, the second, 9(c), referred to the variant with a macro-cell added to simulate the outlier condition.

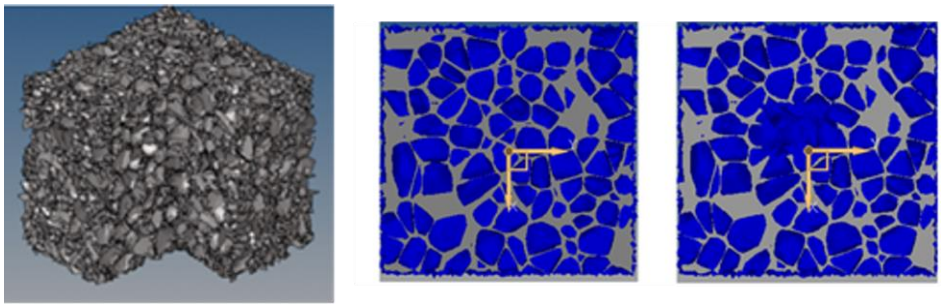

Figure 9: (a) Tetramesh of the final model, (b) section of the original model, (c) its variant with the addition of an outlier (cell with larger volume).

Thanks to the adoption of a Voronoi diagram, the solid model is rather easy to be obtained, since no defeaturing or non-manifold tessellation are present.

Finally, in Figures 10 and 11, an example of the utility of the workflow is provided. Figure 10 shows the results obtained when the two models of Figures 9(b) and 9(c), the original model and its variant, are simulated in a quasi-static crushing condition. The specimen on the right, Figure 10(b),

at the same level of crushing, shows stress concentration due to cavity collapse. This produces a large oscillation in the stress-strain behavior, as shown in Figure 11, where the comparison between experimental curves and their predictive models is shown. Although they are related to specimens taken from the same ingot, with similar nominal and global values, it is evident that cell morphology induces relevant scattering.

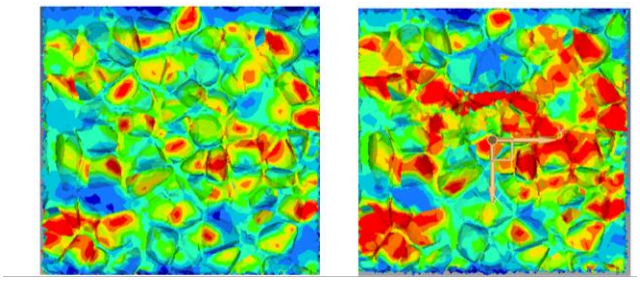

Figure 10: Von Mises stress (max 410 MPa, in red) on sections of Figures 9(b) and 9(c) under crushing.

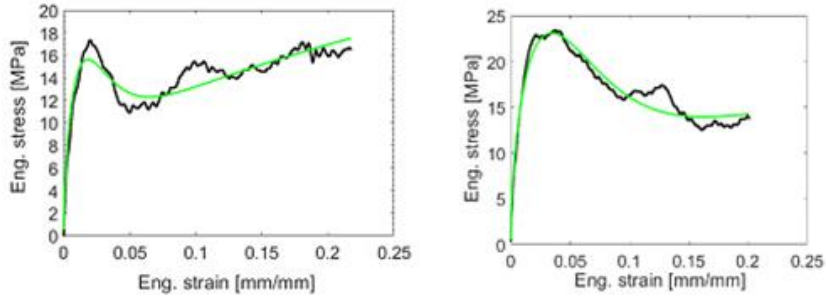

Figure 11: Experimental curves (black) and numerical prediction under crushing of specimens with equal nominal condition but with different presence of outlier cells [11].

5 CONCLUSION

The enhancements of a workflow for FEA modeling of aluminum foam at a mesoscale level have been discussed through examples and sensitivity analysis. The adoption of an iterative procedure based on the Voronoi Diagram, starting from random seeds in a volume conveniently bigger than the effective one, through a scale factor X, has the advantages of avoiding non-manifold tessellation and mesh problems. On the contrary, it requires input parameters, as the scale factor X, suitable to guarantee the correspondence with the requested VVF. Nevertheless, the final model can reproduce a proper distribution of cell morphology by taking into account cell areas and sphericity. Despite tomography allows the reverse engineering of foams to obtain the virtual model of a specimen, the proposed workflow does not aim at reproducing exactly a specimen but it aims at reproducing the statistical dispersion of a set of specimens, so that through FEA analysis a proper computation of the related scattering in the mechanical behavior could be obtained.

Michele Bici, https://orcid.org/0000-0002-7744-2152
Francesca Campana, http://orcid.org/0000-0002-6833-8505
Edoardo Mancini, https://orcid.org/0000-0003-2572-864X

Daniela Pilone, https://orcid.org/0000-0002-8757-8360
Marco Sasso, http://orcid.org/0000-0002-6268-655X

REFERENCES

[1] Ambu, R.; Morabito, A.E.: Design and analysis of tissue engineering scaffolds based on open porous non-stochastic cells, Lecture Notes in Mechanica, 2017, https://doi.org/10.1007/978-3-319-45781-9_78.
[2] Bici, M.; Campana, F.; De Michelis, M.: Mesoscale Modeling of Cellular Materials for Finite Element Analysis, Computer Aided Design & Applications, 14(6), 2017, 760-769. https://doi.org/10.1080/16864360.2017.1287678.
[3] Boschetto, A.; Campana, F.; Pilone, D.: Comparison through image analysis between al foams produced using two different methods, Journal of Materials Engineering and Performance, 23 (2), 2014, pp. 572-580. https://doi.org/10.1007/s11665-013-0745-2.
[4] Campana, F.; Cortese, L.; Pilone, D.: Property variations in large AlSi7 alloy foam ingots, Mat Sci Eng A-Struct, 556, 2012, 400-407. https://doi.org/10.1016/j.msea.2012.07.004.
[5] Campana, F.; Mancini, E.; Pilone, D.; Sasso, M.: Strain rate and density-dependent strength of AlSi7 alloy foams, Mat Sci Eng A-Struct, 651, 2016, 657-667. https://doi.org/10.1016/j.msea.2015.11.007.
[6] De Berg, M.; Cheong, O.; Van Kreveld, M.; Overmars, M.: Computational geometry: Algorithms and applications, 2008, 1-386. DOI: 10.1007/978-3-540-77974-2.
[7] Fang, Q.; Zhang, J.; Zhang, Y.; Liu, J.; Gong, Z.: Mesoscopic investigation of closed-cell aluminum foams on energy absorption capability under impact, Compos Struct, 124, 2015, 409-420. https://doi.org/10.1016/j.compstruct.2015.01.001.
[8] Gil Montoro, G.C.; Abascal, J.L.F.: The Voronoi Polyhedra as Tools for Structure Determination in Simple Disordered Systems, The Journal of Physical Chemistry, 97(16), 1993, 4211-4215.
[9] Kanit, T.; Forest, S.; Galliet, I.; Mounoury, V.; Jeulin D.: Determination of the size of the representative volume element for random composites: statistical and numerical approach, International Journal of Solids and Structures, 40, 2003, 3647–3679. http://dx.doi.org/10.1016/S00207683(03)00143-4.
[10] Liu, J.; He, S.; Zhao, H.; Li, G.; Wang, M.: Experimental investigation on the dynamic behaviour of metal foam: From yield to densification, Int J Imp Eng, 114, 2018, 69-77. https://doi.org/10.1016/j.ijimpeng.2017.12.016.
[11] Mancini, E.; Campana, F.; Pilone, D.; Sasso, M.: Mechanical Testing Of Metallic Foams For 3D Model And Simulation Of Cell Distribution Effects, (accepted for publication in) Proceedings of 23rd International Conference on Material Forming (ESAFORM 2020), Procedia Manufacturing, Elsevier, May 2020.
[12] Simone A.E.; Gibson L.J.: Effect of solid distribution on the stiffness and strength of aluminium foam, Acta Mater, 46, 1998, 2139-2150. https://doi.org/10.1016/S1359-6454(97)00421-7.
[13] Tamburrino, F.; Graziosi, S.; Bordegoni, M.: The design process of additively manufactured mesoscale lattice structures: A review, Journal of Computing and Information Science in Engineering, 18 (4), 2018. https://doi.org/10.1115/1.4040131.
[14] Zhang, X.; Wu, Y.; Tang, L.; Liu, Z.; Jiang, Z.; Liu, Y.; Xi, H.: Modeling and computing parameters of three-dimensional Voronoi models in nonlinear finite element simulation of closed-cell metallic foams, Mechanics of Advanced Materials and Structures, 25(15-16), 2018, 1265-1275. https://doi.org/10.1080/15376494.2016.1190426.
[15] Ulbin, M.; Vesenjak, M.; Borovinšek, M.; Duarte, I.; Higa, Y.; Shimojima, K., Ren, Z.: Detailed Analysis of Closed-Cell Aluminum Alloy Foam Internal Structure Changes during Compressive Deformation, Advanced Engineering Materials, 20 (8), 2018, art. no. 1800164. https://doi.org/10.1002/adem.201800164.